

Native-oxide-confined high-index-contrast $\lambda=1.15 \mu\text{m}$ strain-compensated InGaAs single quantum well ridge waveguide lasers

D. Liang,¹ D. C. Hall,^{1,a)} J. Y.-T. Huang,² G. Tsvid,² and L. J. Mawst²

¹Department of Electrical Engineering, University of Notre Dame, Notre Dame, Indiana 46556, USA

²Department of Electrical and Computer Engineering, University of Wisconsin, Madison, Wisconsin 53706, USA

(Received 20 June 2008; accepted 22 September 2008; published online 22 October 2008)

High performance native-oxide-confined high-index-contrast (HIC) ridge waveguide (RWG) diode lasers are fabricated in a strain-compensated $\text{In}_{0.4}\text{Ga}_{0.6}\text{As}$ single quantum well structure by employing a deep dry etch plus nonselective O_2 -enhanced wet thermal oxidation process. The thermal native oxide grown on the etch-exposed RWG sidewalls of the $\text{Al}_{0.74}\text{Ga}_{0.26}\text{As}$ waveguide cladding layers and GaAs core with GaAsP-InGaAs quantum well provides both strong optical and electrical confinements for the active region. Due to a smoothing of sidewall roughness by the O_2 -enhanced oxidation, the lasers exhibit a low internal loss in $\alpha_i=7.2 \text{ cm}^{-1}$ for a $w=7.2 \mu\text{m}$ narrow stripe HIC RWG structure, only 53% larger than that of $w=87.2 \mu\text{m}$ broad-area devices, enabling their room temperature operation at a low 300 A/cm^2 threshold current density. © 2008 American Institute of Physics. [DOI: 10.1063/1.3001587]

Highly strained InGaAs quantum well heterostructure (QWH) active regions allow extremely low threshold current density lasers ($J_{\text{th}} < 90 \text{ A/cm}^2$) with wavelengths approaching the $1.2 \mu\text{m}$ region.¹ The high compressive strain of the InGaAs can be effectively compensated by tensile-strained GaAsP or InGaP strain compensation layers.^{2,3} We have previously demonstrated high performance high-index-contrast (HIC) ridge waveguide (RWG) edge-emitting lasers fabricated from $\lambda=808 \text{ nm}$ of InAlGaAs and $\lambda=1.234 \mu\text{m}$ of InGaAsN QW structures⁴ using a modified, O_2 -enhanced wet thermal oxidation process,⁵ which enables the conversion of low Al-content $\text{Al}_x\text{Ga}_{1-x}\text{As}$ ($x < 0.6$) and Al-free GaAs, GaAsP, and InGaAsN into their native oxides. This nonselective oxidation of the entire sidewall of a RWG, etched to below the active region/heterostructure waveguide core, yields a HIC ($\Delta n \sim 1.7$) structure that simultaneously provides electrical confinement with low interface recombination, the elimination of current spreading, and strong optical mode confinement, thus resulting in significant edge-emitting laser performance improvements.^{4,6}

In this letter, we demonstrate the application of this nonselective oxidation process⁵ to an Al-free $\text{In}_{0.4}\text{Ga}_{0.6}\text{As}$ QWH with $\text{GaAs}_{0.85}\text{P}_{0.15}$ strain-compensation layers and a GaAs waveguide core. While we have previously reported the oxidation of an Al-free InGaAsN/GaAsP active region within a GaAs waveguide,⁶ the results in the present work further confirm the capability of nonselective oxidation in forming native oxides on various Al-free III-As compound semiconductors (i.e., InGaAs, GaAs, and GaAsP). This is because the dimethylhydrazine (DMHy) source used for N incorporation during InGaAsN growth is not used here and thus the possible interaction between DMHy and Al in the metal-organic chemical vapor deposition (MOCVD) reactor, which may have previously led to Al incorporation into these oxidized layers, is therefore eliminated in this work. We also present sidewall oxidation depth versus time data at various positions in the heterostructure to show the role of vertical oxi-

dation from heterointerfaces in achieving a relatively uniform oxide thickness up and down the ridge sidewall. Finally, HIC RWG lasers are demonstrated with low threshold current densities ($82.6 \text{ A/cm}^2 < J_{\text{th}} < 287.3 \text{ A/cm}^2$), high current injection efficiency ($88.6\% > \eta_i > 77.4\%$), and low internal loss ($4.7 \text{ cm}^{-1} < \alpha_i < 7.2 \text{ cm}^{-1}$) over all broad-area and narrow-stripe devices with a width range of $147 \mu\text{m} > w > 7.2 \mu\text{m}$, respectively. The narrowest lasers in this work show a five to sixfold improvement in output power and threshold current density over the InGaAsN QWH lasers in Ref. 6, demonstrating that very high-performance devices can be realized by this process. Kink-free operation with the absence of thermal roll over is observed for unbonded, p -side up devices at injection currents up to $27.6\times$ and $10.3\times$ threshold in pulsed (10 kHz) and fast-dc modes, respectively.

The laser QWH in this work (Fig. 1 insert) is grown by low-pressure MOCVD as in Ref. 1. The highly lattice mis-

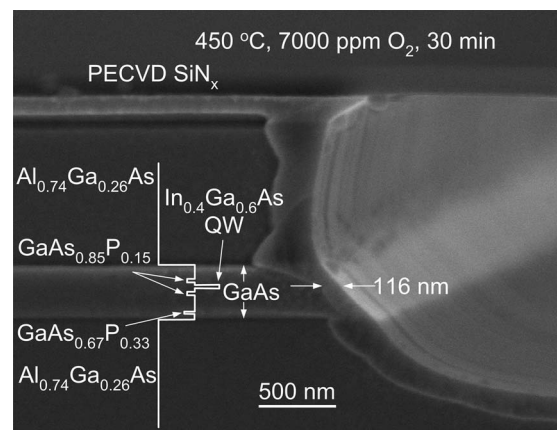


FIG. 1. SEM cross-section image of $w=15 \mu\text{m}$ $\text{In}_{0.4}\text{Ga}_{0.6}\text{As}$ SQW structure, wet etched and nonselectively oxidized at $450 \text{ }^\circ\text{C}$ with 7000 ppm O_2 participation for 30 min, showing 116 nm oxide growth in $\text{In}_{0.4}\text{Ga}_{0.6}\text{As}$ active region. The inset conduction band schematic highlights the epitaxial structure.

^{a)}Electronic mail: dhall@nd.edu.

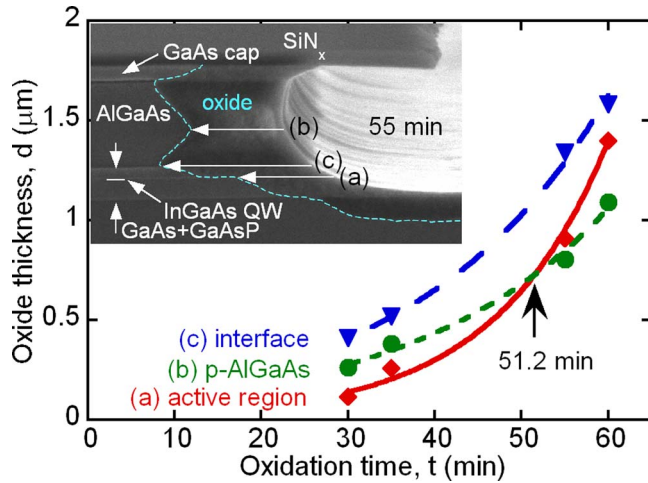


FIG. 2. (Color online) Native oxide thickness at (a) InGaAs active region, (b) p -AlGaAs, and (c) AlGaAs/GaAs interface vs oxidation time with exponential fit. Inset: SEM cross-sectional image of a wet-etched stripe oxidized 55 min at 450 °C with 7000 ppm O_2 , with oxidation front highlighted by dashed line.

matched 60 Å $In_{0.4}Ga_{0.6}As$ single QW (SQW) is located 100 nm below a 1.1 μm p - $Al_{0.74}Ga_{0.26}As$ upper cladding, asymmetrically within a 300 nm unintentionally doped GaAs waveguide layer. Two 75 Å $GaAs_{0.85}P_{0.15}$ tensile-strained barriers on each side of the QW reduce the effective strain from the $In_{0.4}Ga_{0.6}As$, and significantly improve the laser performance, particularly in the presence of high Al-content cladding layers.^{3,7} A 27 Å $GaAs_{0.67}P_{0.33}$ tensile strain buffer is also inserted between the GaAs waveguide layer and the 1.1 μm n - $Al_{0.74}Ga_{0.26}As$ lower cladding layer.^{3,7}

The nonselective oxidation⁵ of the InGaAs SQW active region and GaAs waveguide layer is first studied on wet-etched ridges. The scanning electron microscope (SEM) image in Fig. 1 shows the sidewall of a 15 μm wide plasma-enhanced chemical vapor deposition SiN_x -masked ridge wet-etched in a $H_3PO_4:H_2O_2:H_2O$ solution for 90 s. When wet oxidized for 30 min at 450 °C with the addition of 7000 ppm O_2 (relative to the N_2 carrier gas bubbled through 95 °C H_2O), approximately 116 nm of oxide grows at the $In_{0.4}Ga_{0.6}As$ QW position. The lateral oxidation depth for times of 30, 35, 55, and 60 min is plotted in Fig. 2 at the positions of (a) the InGaAs QW, (b) the center of the p -AlGaAs layer, and (c) the GaAs core/ p -AlGaAs cladding layer interface. Comparing the SEM images at 30 min (Fig. 1) and at 55 min (Fig. 2 inset), we observe the formation of an anisotropic “spike” in the oxidation front at the GaAs WG core/ p -AlGaAs cladding interface, growing exponentially with time. This effect has been attributed to an anodic charging effect due to blackbody radiation-induced photogeneration of electron-hole pairs, separated by the built-in field of the p - n heterojunction.⁸ Vertical oxidation subsequently proceeds isotropically from the porous native oxide spike forming at the interface, resulting in an effective enhancement in the lateral oxidation rate of the adjoining material, which lessens at increased distance from the interface. The oxidation spike at the top interface between the upper p -AlGaAs cladding and the p^+ -GaAs cap may also be explained by the anodic charging effect,⁸ with carriers separated by the built-in field existing due to heterointerface band realignment.

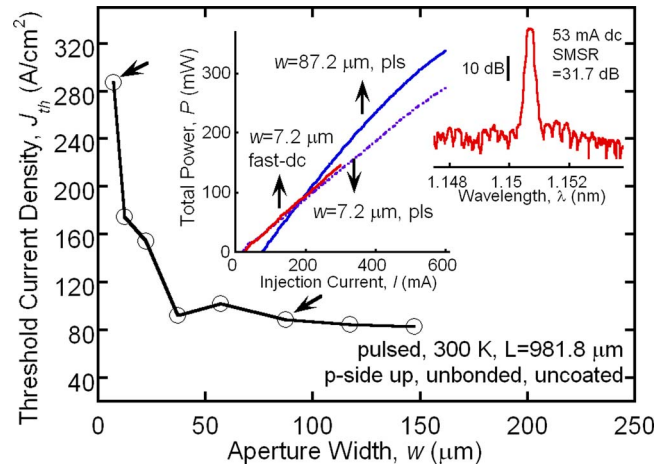


FIG. 3. (Color online) Pulsed J_{th} vs effective laser aperture width w for HIC RWG lasers with $L=982$ μm. Left inset: Total (2-facet) output power vs current of $L=982$ μm devices with $w=7.2$ μm [pulsed (“pls”) and fast dc] and $w=87.2$ μm (pulsed). Right inset: Logarithmic scale single longitudinal mode spectrum of $w=7.2$ μm laser at $I=53$ mA CW.

Figure 2(c) shows that the oxide growth is most rapid at the GaAs/ p -AlGaAs interface, and subsequently enhances the apparent lateral oxidation rate at both (a) the InGaAs QW active region and (b) the middle of the upper AlGaAs cladding. Due to its closer vicinity to the GaAs/ p -AlGaAs interface, the oxide thickness at the InGaAs active region exceeds that at the p -AlGaAs cladding center after 51.2 min according to the crossing point of exponential fits to the data in Fig. 2. The above mechanism clearly plays an important role in making O_2 -enhanced oxidation of heterostructures⁵ effectively “nonselective” so that a relatively uniform thickness oxide can be grown on the RWG sidewall.

Deeply etched HIC RWG laser diodes with mask stripe widths w varying from 10 to 150 μm are fabricated using Cl-based reactive ion etching as in Ref. 6 in order to achieve better dimensional control. After a 1 h nonselective wet oxidation with the addition of 7000 ppm O_2 , a 1.4 μm thick native oxide is formed at the QW active region [Fig. 2(a)]. All devices are unbonded (i.e., with no heatsinking employed) and are probe tested p -side up in pulsed (1 μs and 1% duty cycle), fast-dc (typically 0.4 s dc sweep), and continuous-wave (CW) modes at 300 K. Figure 3 shows the pulsed, 300 K J_{th} versus w for a set of HIC RWG lasers from the same $L=981.8$ μm bar. Notably, J_{th} at $w=7.2$ μm is just 3.5× higher than that of a $w=147.2$ μm broad-area device, indicating excellent electrical and optical confinements, with low nonradiative recombination even with a III-V native oxide grown in direct contact with the active region. Conventional $w=5$ μm weak-index-contrast RWG lasers, in which a shallow etch stops above the active region in the upper cladding layer, show a 2.3× higher J_{th} than oxide-confined HIC devices due to severe lateral current spreading.⁶ Despite possible nonradiative current leakage at the oxide-semiconductor interface, the HIC RWG structure results in the best overall narrow stripe laser performance because of its strong optical and electrical confinement.

The left inset of Fig. 3 shows total light output power versus current (L - I) characteristics of two representative, $w=7.2$ and 87.2 μm, devices from a $L=982$ μm bar. For the $w=7.2$ μm device, no thermally induced roll over is observed up to an output power of 276 mW at 600 mA (27.5

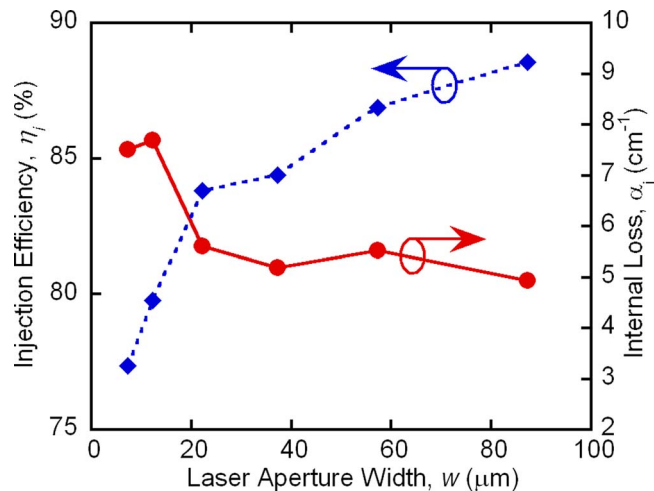


FIG. 4. (Color online) Internal loss α_i and injection efficiency η_i vs laser aperture width w .

times above the $I_{\text{th}}=21.8$ mA threshold) in pulsed mode and up to 149 mW at 300 mA (10.3 times above the $I_{\text{th}}=29.0$ mA threshold) in fast-dc mode, both with a slope efficiency of 0.54 W/A. The $w=87.2$ μm device shows a threshold of 75 mA and an initial slope efficiency of 0.83 W/A with pulsed operation up to 340 mW at 600 mA ($8\times$ threshold and only slight thermal rollover). The close proximity of the active region and the Ti+Au metalized oxidized ridge sidewalls provides excellent heat dissipation for these unbonded lasers. Operation at higher injection levels was avoided to protect the uncoated device facets. The uniform distribution of injected carriers in the HIC RWG structure, where current spreading is eliminated, leads to the uniform simultaneous excitation of all supported waveguide modes regardless of the stripe width, suppressing mode competition and resulting in clean kink-free operation to high drive currents. The log scale output spectrum (right inset in Fig. 3) for a $w=7.2$ μm device measured at 53 mA CW shows a peak emission wavelength of 1.1507 μm . Further investigation is needed to understand the origin of the observed single longitudinal mode operation with high side-mode suppression ratio (SMSR) of 31.7 dB, unusual for a Fabry-Pérot resonator, and to fully characterize output beam and spectral properties for heatsunk lasers under CW conditions. Single spatial mode operation of up to 40 mW CW has been reported elsewhere for similar unbonded 808 nm HIC RWG lasers.⁴

The device internal loss α_i and internal (injection) efficiency η_i are extracted from a linear regression fitting of the inverse external quantum efficiency versus cavity length data for 3–5 cavity lengths at each width. Figure 4 shows the α_i and η_i versus laser aperture size w , where $\alpha_i \leq 7.3$ cm^{-1} and $\eta_i > 77.4\%$ is achieved on all devices. While increased non-radiative sidewall recombination can reduce η_i if the carrier density outside the QW active region remains unclamped above threshold,⁹ the decrease in η_i as w decreases is not necessarily indicative of such. Rather, the inverse relationship between the α_i and η_i versus w data may suggest a reduced efficiency in the injection and collection of carriers

by the QW as the higher α_i requires higher gains and, thus, higher carrier densities. At these higher pumping levels, the scattering of higher-energy carriers into the well becomes less efficient and/or carriers may overflow into other higher-energy leakage paths. The HIC waveguide scattering loss increases exponentially with the reduction in w due to strong field interactions with the etched + oxidized sidewall roughness.¹⁰ In these lasers, absorption of the field by the electrode metals deposited on top of the native oxide is considered negligible as the 1.4 μm oxide thickness is >23 times thicker than the simulated $1/e$ skin depth of ~ 60 nm for the evanescent field within the oxide. One of the most significant benefits of the HIC RWG process utilized here is the concomitant sidewall roughness smoothing provided by the oxygen-enhanced wet thermal oxidation process.^{11,12} Though the total laser loss is comprised not only of sidewall scattering, but also free carrier absorption, interface scattering, and other losses, the increase in loss here from $\alpha_i=4.7$ to only 7.2 cm^{-1} (just $\sim 53\%$) when scaling the ridge width from $w=87.2$ to 7.2 μm is notable. This result suggests that the oxidation smoothing of the dry-etched sidewall (defined via nonoptimized contact lithography as in Refs. 11 and 12) indeed substantially reduces the impact of sidewall scattering in the total waveguide loss and contributes to the high performance of these lasers.

We have demonstrated that the oxidation of Al-free $\text{In}_{0.4}\text{Ga}_{0.6}\text{As}$ QW, GaAsP barrier, and GaAs waveguide layers can be achieved through a modified O_2 -enhanced wet thermal process. Apparent anodic charging-enhanced oxidation at nearby heterojunctions and interfaces is shown to impact the nonselectivity of heterostructure sidewall oxidation and corresponding ability to grow a relatively uniform oxide film. The resulting high-quality native oxide enables the realization of high-performance $\lambda=1.15$ μm HIC RWG lasers with low threshold current density, low internal loss, high efficiency, a large SMSR, and kink-free operation to high output powers.

The authors gratefully acknowledge the support of National Science Foundation Award No. ECS-0601702.

- ¹N. Tansu, J. Y. Yeh, and L. J. Mawst, *J. Appl. Phys.* **82**, 4038 (2003).
- ²Won-Jin. Choi, P. D. Dapkus, and J. J. Jewell, *IEEE Photon. Technol. Lett.* **11**, 1572 (1999).
- ³N. Tansu and L. J. Mawst, *IEEE Photon. Technol. Lett.* **13**, 179 (2001).
- ⁴D. Liang, J. Wang, and D. C. Hall, *Electron. Lett.* **42**, 349 (2006).
- ⁵Y. Luo and D. C. Hall, *IEEE J. Sel. Top. Quantum Electron.* **11**, 1284 (2005).
- ⁶D. Liang, J. Wang, J. Y.-T. Huang, J.-Y. Yeh, L. J. Mawst, and D. C. Hall, *IEEE J. Sel. Top. Quantum Electron.* **13**, 1324 (2007).
- ⁷N. Tansu and L. J. Mawst, *IEEE Photon. Technol. Lett.* **14**, 444 (2002).
- ⁸S. A. Maranowski, N. Holonyak, Jr., T. A. Richard, and F. A. Kish, *Appl. Phys. Lett.* **62**, 2087 (1993).
- ⁹L. A. Coldren and S. W. Corzine, *Diode Lasers and Photonic Integrated Circuits* (Wiley, New York, 1995), pp. 425–427.
- ¹⁰K. K. Lee, D. R. Lim, H.-C. Luan, A. Agarwal, J. Foresi, and L. C. Kimerling, *Appl. Phys. Lett.* **77**, 1617 (2000).
- ¹¹D. Liang and D. C. Hall, *Appl. Phys. Lett.* **91**, 061110 (2007).
- ¹²C. S. Seibert, D. Liang, D. C. Hall, and Z. A. Shellenbarger, 2008 Conference on Lasers and Electro-Optics, San Jose, CA, 2008, Paper No. JTuA22.